Universe Scientific Publishing

Clean Energy Science and Technology 2024, 2(3), 188.
https://doi.org/10.18686/cest.v2i3.188

Article

Effect of temperature on water evaporation coefficient (E) in a thermobalance: A solar-driven steam generation approach

Carlos Enrique Rojas-Sánchez, Rodolfo Antonio Hernández-Chaverri*

Laboratorio de Ingeniería en Bioprocesos (LIBP), Universidad Estatal a Distancia, Palmares 20701, Costa Rica
*** Corresponding author:** Rodolfo Antonio Hernández Chaverri, rohernandez@uned.ac.cr

CITATION

Rojas-Sánchez CE, Hernández-Chaverri RA. Effect of temperature on water evaporation coefficient (E) in a thermobalance: A solar-driven steam generation approach. Clean Energy Science and Technology. 2024; 2(3): 188. https://doi.org/10.18686/cest.v2i3.188

ARTICLE INFO

Received: 16 July 2024
Accepted: 20 September 2024
Available online: 23 September 2024

Abstract: During this investigation, the variation of the water evaporation phenomenon with the defined drying temperature and mass of water was analyzed, five levels were studied (50, 60, 70, 80 and 90 ℃), finally a correlation between temperature and evaporation rate was generated. With the study carried out, it was defined that the water evaporation velocity can be calculated with an initial mass of 35 g at 90 ℃, while the necessary time for the determination was 120 min. In addition, it was determined that the evaporation velocity follows a quadratic behavior with temperature, according to the experiments carried out with the Sartorius MA-100 balance, while the maximum deviation recorded was 0.349 mmol/m^{2}s for a temperature of 80 ℃. It is concluded that the determination of the water evaporation velocity is highly dependent on the temperature and mass of water. Furthermore, this study can be used as a basis for future studies aimed at improving the efficiency of processes such as steam and electricity cogeneration.

Keywords: evaporation; water; temperature; moisture analyzer; steam; generation

1. Introduction

The global dependence on fossil fuels and the scarcity of drinking water in various parts of the planet underscore the growing demand for sustainable alternatives to address these issues [1]. In response, organizations like the United Nations have defined an action path through the Sustainable Development Goals, highlighting affordable and clean energy, sustainable cities and communities, and clean water and sanitation.

This situation has driven the development of technologies that efficiently harness solar energy, one of which is photothermal cogeneration of steam and electricity [2–4]. However, volumetric heating has a solar-to-steam conversion efficiency of around 40% [5]. As a result, this technology is being directed toward interfacial solar steam generation, which increases efficiency values [6–8].

This technology is based on photothermal and photoelectric principles, where heat generated by solar radiation is used to produce steam, while the temperature difference between evaporation and a thermoelectric generator enables electricity generation [9,10]. Additionally, the condensation of the produced steam can be used as a water purification strategy [11–13].

In this context, there is a need to seek conditions and technologies that increase the efficiency of both processes. This research focuses on the effect of variables such as time, water mass or height, and temperature on the water evaporation rate. For this, a moisture balance with an infrared resistance as a heating source was used. The aim is to contribute to the development and design of cogeneration systems.

The rate of water vaporization over a hot surface depends on large number of factors, among the most relevant are: the environmental conditions (temperature, barometric pressure and relative humidity), heat transfer area, shape of sample container, impurities, and vapor pressure at the analyzed temperature [14–20].

Evaluating the water evaporation process over time in a thermobalance, it's learned that the amount of vaporized water has a mainly linear behavior, as can be seen in **Figure 1**, which marks three different zones: a) conditioning zone, where the system reaches to the selected temperature, b) linear zone, defined by a proportional relation and c) non-linear zone, caused by formation of islands on the plate without the presence of liquid [21,22].

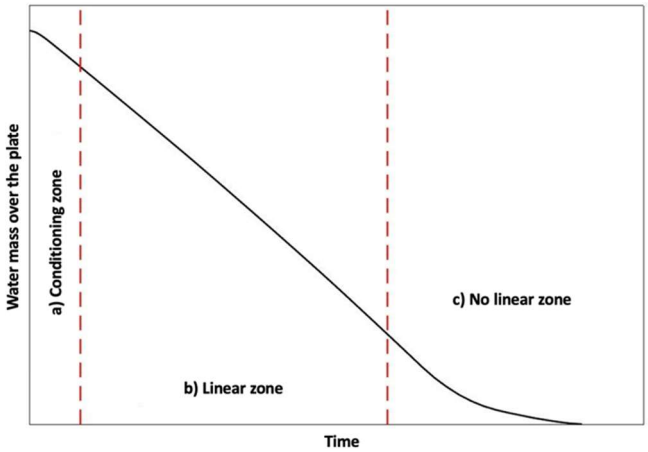

Figure 1. Water mass behavior vs time in a thermobalance.

2. Materials and methods

2.1. Calculation of the drying area

Tests were carried out using 80x aluminum pan (Sartorius, 6965542) with an average diameter of 90 mm, however, they have a conical shape, as can be seen in **Figure 2**. Therefore, the drying area varies with the height of the liquid in the pan. For this reason, a variable drying area was defined according to the water mass in a p at time t.

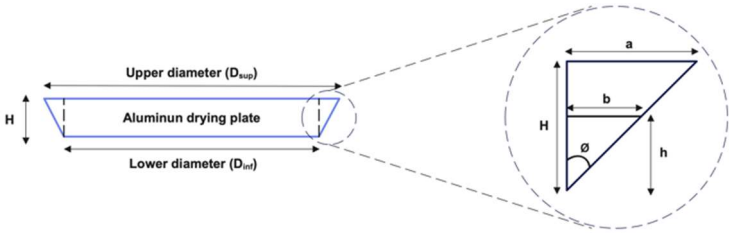

Figure 2. Diagram of 80x aluminum weighing pan (Sartorius).

Firstly, a representative sample of pan was taken (n = 20), upper diameter (D_{sup}), lower diameter (D_{inf}), and height (H) was measured; with the collected values, a relation between diameter and water mass in the pan at moment t was proposed, as detailed below.

The relation between diameter and water mass in pan was calculated using $\emptyset$ (Equation (1)):

$$\emptyset = \arctan\left(\frac{a}{H}\right) = \arctan\left(\frac{D_{sup} - D_{inf}}{H \cdot 2}\right) \quad (1)$$

Then, b was calculated (Equation (2)). ρ_T is water density at T temperature.

$$3 \cdot \frac{m(t)}{\rho_T} \cdot \tan\emptyset \cdot \frac{4}{\pi} = 4 \cdot b(t)^3 + 6 \cdot D_{inf} \cdot b(t)^2 + 3 \cdot D_{inf}^2 \cdot b(t) \quad (2)$$

Finally, drying area at t moment ($A_s(t)$) was calculated (Equation (3)):

$$A_s(t) = \frac{\pi \cdot \left(2 \cdot b(t) + D_{inf}\right)}{4} \quad (3)$$

Distilled water was used in all analyses. In this section, the maximum variation between the recommended adjustment in the present study and constant area assumption for different volumes was estimated.

2.2. Water evaporation coefficient determination

Moisture analyzers were programmed, and standard drying was set. In each experiment, temperature was selected, and water mass was registered vs. drying time. Also, barometric pressure, relative humidity, and room temperature were measured. With the resulting data, the amount of water by unit area ($n_w(t)$) was calculated for each time, which can be seen in Equation (4), MM_w is the water molecular mass.

$$n_w(t) = \frac{m(t)}{MM_w \cdot A_s(t)} \quad (4)$$

Then, $n_w(t)$ was analyzed vs time. Water evaporation coefficient presents a linear zone slope, as can be observed in the next expression (Equation (5)):

$$E = \frac{-dn_w/dt}{A_s} \quad (5)$$

2.3. Initial water mass effect in water evaporation coefficient

This study was performed at 90 ℃, superior temperature limit of this investigation. Three mass levels were defined: 15 g, 25 g, and 35 g. Finally, water evaporation coefficient was calculated for each case. These assays were executed in Sartorius MA-100 thermobalance.

2.4. Analysis time effect in water evaporation coefficient determination

In further stages, the evaporation of 35 g of water was performed using two temperatures: 50 ℃ and 90 ℃ with Sartorius MA-100 thermobalance. Assays were concluded when water mass variation was less than 1 mg in 5 min.

2.5. Temperature effect in water evaporation coefficient determination

Additionally, temperature effect was studied. Water evaporation coefficient was determined (by quintupled) for five temperatures (50 ℃, 60 ℃, 70 ℃, 80 ℃, and 90 ℃) using a time of 120 min and initial water mass of 35 g. Sartorius MA-100 and OHAUS MB 120 were used.

3. Results and discussion

First off, maximum percentage variation between proposed drying area and constant area assumption (using manufacturer reported nominal diameter) was calculated for different initial volumes (full pan, 35 mL, 25 mL, 15 mL), also, divergence in E determination (**Table 1**).

Table 1. Maximum percentage area and E variation for different initial volumes.

Initial volume (mL)	Maximum percentage area variation (%)	Maximum percentage E variation (%)
Full pan	21.90	17.97
35	19.06	16.01
25	17.04	14.56
15	15.00	13.04

The greater the amount of water added initially, bigger the maximum percentage variation of area and E were found (21.90 % and 17.97 % for full pan, respectively). This situation shows that dynamic area approximation is necessary because variation was not depreciable (overcome divergences of 10 % for both performed calculations).

Consecutively, a preliminary study of water evaporation phenomenon for different temperatures (50 °C, 60 °C, 70 °C, 80 °C, and 90 °C) was performed, conditions frequently reached in solar-assisted evaporation systems, using Sartorius MA-100, with a room temperature that varied between 22.2 °C and 28.8 °C, relative humidity between 55.9 % and 77.0 % and altitude of 1000 m. The objective was to know the amount of water over the pan versus the time until the water reached evaporation. The temperature reached in various solar steam generation processes vary depending on the research conditions and approach. However, values between 50 °C and 165 °C have been recorded [23–30].

In **Figure 3**, the obtained behavior for each analyzed temperature can be seen. In each case, the same pattern was observed and could recognize the three zones marked in **Figure 1**. Additionally, emphasizing limit temperature values, 50 °C, and 90 °C, the necessary time for total evaporation of water at 50 °C was four times higher than at 90 °C. Therefore, temperature increase represents an evaporation time decrease, or an evaporation rate increment [21].

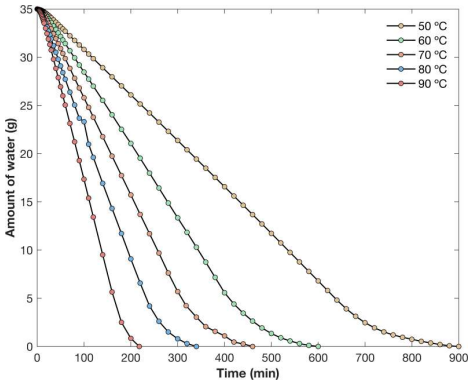

Figure 3. Amount of water versus time for different temperatures, using Sartorius MA-100.

Also noteworthily, (**Figure 3**) the lower the temperatures the wider marked zones, hence at 50 ℃ it's necessary a higher time of stabilization or conditioning to start the linear behavior. This phenomenon can be explained by a lower difference between analysis temperature and room temperature [31].

Evaporation processes occur mainly in linear zones such as can be seen for all temperatures; thus, it's crucial to focus on this part of evaporation phenomenon. Established the linear zone as the principal interest of the study, evaporation water coefficient was determined, it corresponds to the negative of linear zone slope (Equation (5)).

For cogeneration of steam and electricity through solar energy, it is advisable to operate in a zone of constant velocity, ensuring that the water height is not a limiting factor in the evaporative process. Currently, the design of cogeneration evaporators is focused on 3D configurations, modifying the water transport height, reaching up to 15 cm [32], with the aim of increasing the efficiency of the steam generation process [33,34] .

Consecutively, the initial water mass influence of E determination was studied. Three assays (35 g, 25 g and 15 g) were performed at 90 ℃, superior temperature used in the study, with an analysis time of 120 min (**Figure 4**).

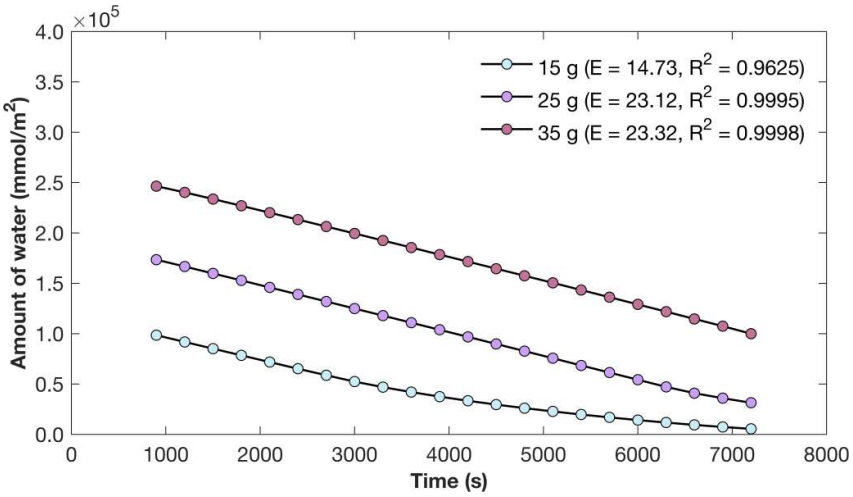

Figure 4. Amount of water versus time for different initial mass of water, using Sartorius MA-100.

Figure 4 shows a proportional relation; therefore, with initial mass diminution, correlates a decrease in the linear zone time, for instance, if the initial mass is 15 g, the linear behavior stays around 40 min, and for 35 g, the linear zone reaches 120 min.

If linear adjustment between 15 min and 120 min for each initial mass, can be see a reduction of R^2. and E with water mass decrease. This fact can be explained by an evaporative phenomenon limitation supported by water film break over aluminum plate, forming regions without water presence (islands, **Figure 5**). For the next assays 35 g of water was selected foreseeing high evaporation rates. These assays were performed with a room temperature that varied between 27.3 ℃ and 30.0 ℃, and relative humidity between 55.2 % and 59.8 %.

Figure 5. Island formation without water presence.

Thereafter, the effect of analysis time was studied, comparing the evaporation of 35 g water at 50 ℃ and 90 ℃ (**Figure 6**). In both scenarios, the linear behavior was maintained almost all the time, however, 90 ℃ was selected to define assay time and normalize tests. In this case, the linear zone was delimited between 15 min and 120 min achieving a correlation coefficient of 0,9997. For the same range but at 50 ℃ the correlation coefficient was 0.9996. At all events, a R^2 higher than 0.9995 was sought.

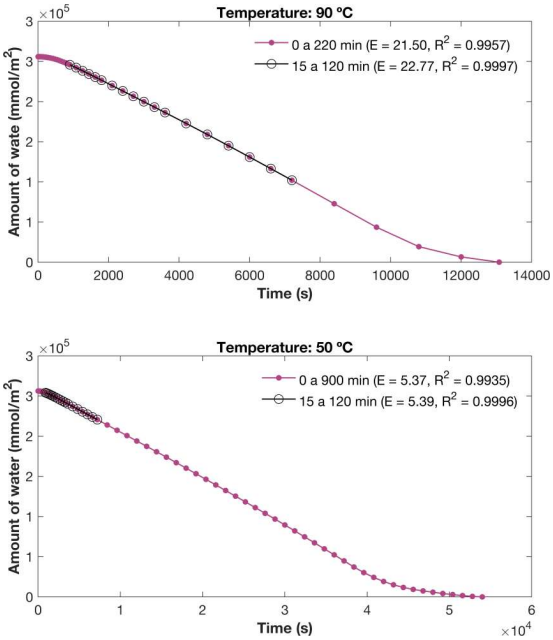

Figure 6. Amount of water versus time at 50 ℃ and 90 ℃, using Sartorius MA-100.

The necessary time for E determination is directly related to the initial mass of water. The time and initial water mass were 120 min and 35 g, respectively, looking for a regression adjustment with a R^2 superior to 0.9995. Therefore, an accurate determination of E must consider the conditioning of the system as it reaches the working temperature and must ensure that there is no lack of water at any point in the process, as this would result in a decrease in evaporation efficiency.

Then proceeding, a study of temperature and its effect in E determination was carried out. Five temperatures were selected (50 ℃, 60 ℃, 70 ℃, 80 ℃ and 90 ℃), conditions easily reached in solar cogeneration systems. All assays were performed quintupled using Sartorius MA-100 (BH1). These tests were performed with a room

temperature that varied between 21.9 ℃ and 29.8 ℃, relative humidity between 45.1 % and 78.1 % and altitude of 1000 m.

Temperature increase means an increment of vaporization rate and E (**Figure 7**). This behavior can be explained in terms of heat transfer, however with temperature rise more heat is generated, accelerating sample evaporation [21].

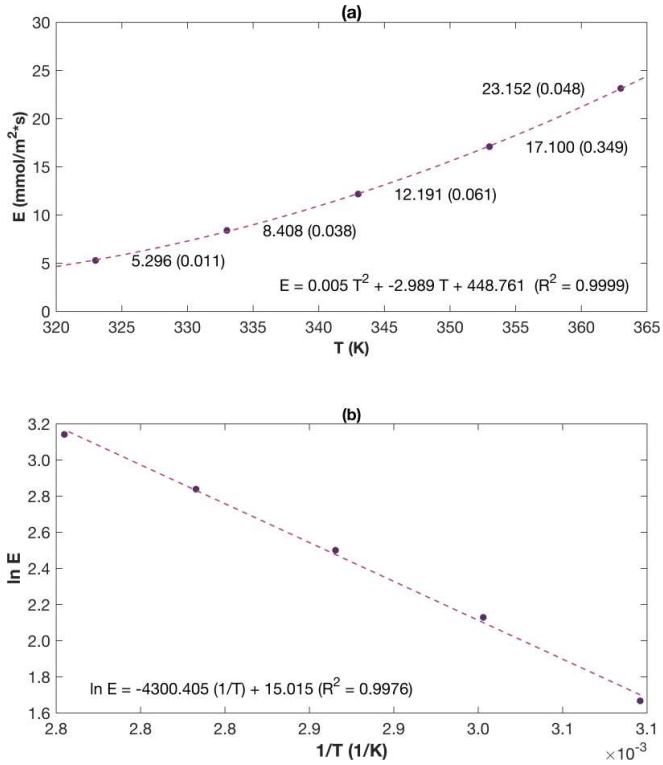

Figure 7. E relation with temperature, using Sartorius MA-100. **(a)** second grade polynomic adjustment; **(b)** Arrhenius adjustment.

Additionally, with the increase in temperature, the water vapor pressure rises, allowing for faster evaporation, as the kinetic energy of the molecules increases, enabling their escape from the liquid phase to the gaseous phase. This situation explains the need to implement strategies that enhance solar conversion efficiency, such as the design of two-dimensional or three-dimensional evaporators. If the goal is to desalinate sea water, the strongest natural ocean evaporation rate occurs in tropical belt (10° S and 20° S), with an estimated evaporation rate of 1540 mm/year (0.00271 mmol/m^2·s) [35] and the ocean average world temperature is 17 ℃ (with maximum of 35 ℃) [36,37].

Disregarding the influence of relevant factors such as the presence of salts, the effect of wind on evaporation, or the inconsistency of solar radiation, it is important to highlight the need to search for technologies that enhance heat transfer and increase steam generation efficiency. It is also crucial to note the significant difference in the evaporation rate previously mentioned for seawater and the rate achieved with the equipment under controlled temperature conditions and constant radiation.

According to Djellabi et al. [38], various studies on steam generation from sunlight are presented, where water evaporation rates between 49.6 and 14.4

mmol/m²·s with efficiencies above 70 % are found, exemplifying how promising these technologies are for electricity cogeneration and water treatment.

E deviations were found between 0.01 mmol/m^2 s and 0.35 mmol/m^2 s. The maximum calculated deviation was obtained at 80 °C, that represents 2 % of E value for this temperature (17.100 mmol/m^2 s). This situation allows to infer that room temperature and relative humidity do not affect E determination for each temperature.

Additionally, the relation between water evaporation coefficient and temperature was adjusted using second grade polynomial equation, with a R^2 of 0.9999, thereupon the existence of a quadratic behavior that can be seen in Equation (6).

$$E = 0.005 \cdot T^2 - 2.989 \cdot T + 448.761 \quad (6)$$

Another method to adjust the data consists in linearized Arrhenius equation (Equation (7)):

$$\ln E = 15 - 4300.4 \cdot \frac{1}{T} \quad (7)$$

A correlation coefficient of 0.9976 was obtained. The activation energy was 35.753 kJ/mol. This value can be associated with the amount of solar energy needed to initiate the water evaporation process under the studied conditions, and therefore, it can be used as a reference for determining the required solar energy to carry out the process, as well as for determining the efficiency.

4. Conclusion

The present study emphasizes that temperature is a determining factor in the variation of the water evaporation rate (E), which can be applied in steam generation systems using solar energy to improve operational efficiency. The results show that as the temperature increases, water evaporation also increases, following a quadratic relationship. Additionally, recommendations are made regarding the calculation of the water evaporation rate, a crucial variable in determining the efficiency of solar generation systems.

On the other hand, care must be taken with the amount of water during the process, as if the water level is too low, the evaporation rate begins to decrease significantly. Therefore, it is important to ensure that the water level in steam generation systems is never a limiting factor in the process.

For future studies, it is recommended to investigate variables such as wind speed, the inconsistency of solar radiation, and the implementation of impurities such as salts in the water, and to examine their effect on the water evaporation rate.

Author contributions: Conceptualization, CERS and RAHC; methodology, CERS and RAHC; software, CERS and RAHC; validation, CERS and RAHC; formal analysis, CERS; investigation, CERS and RAHC; resources, CERS and RAHC; data curation, CERS; writing—original draft preparation, CERS and RAHC; writing—review and editing, CERS and RAHC; visualization, CERS; supervision, RAHC; project administration, RAHC; funding acquisition, CERS and RAHC. All authors have read and agreed to the published version of the manuscript.

Acknowledgments: Dr. Julio Mata Segreda by revision and sugerences.

Conflict of interest: The authors declare no conflict of interest.

References

1. Li X, Xie W, Zhu J. Interfacial solar steam/vapor generation for heating and cooling. Advanced Science. 2022; 9(6): e2104181. doi: 10.1002/advs.202104181
2. Ren J, Ding Y, Gong J, et al. Simultaneous Solar-driven Steam and Electricity Generation by Cost-effective, Easy Scale-up MnO_2-based Flexible Membranes. Energy & Environmental Materials. 2023; 6(3): e12376. doi: 10.1002/eem2.12376
3. Huang L, Wang Y, He R, et al. Solar-driven co-generation of electricity and water by evaporation cooling. Desalination. 2020; 488: 114533. doi: 10.1016/j.desal.2020.114533
4. Xu Y, Dong S, Sheng Y, et al. Highly efficient solar driven cogeneration of freshwater and electricity. Journal of Materials Chemistry A. 2023; 11(4): 1866-1876. doi: 10.1039/D2TA08590A
5. Li X, Cooper T, Xie W, Hsu PC. Design and utilization of infrared light for interfacial solar water purification. ACS Energy Letters. 2021; 6(8): 2645-2657. doi: 10.1021/acsenergylett.1c00869
6. Xie Z, Duo Y, Lin Z, et al. The rise of 2D photothermal materials beyond graphene for clean water production. Advanced Science. 2020; 7(5): 1902236. doi: 10.1002/advs.201902236
7. Li Z, Ma X, Chen D, et al. Polyaniline-coated MOFs nanorod arrays for efficient evaporation-driven electricity generation and solar steam desalination. Advanced Science. 2021; 8(7): 2004552. doi: 10.1002/advs.202004552
8. Alvarez PJJ, Chan CK, Elimelech M, et al. Emerging opportunities for nanotechnology to enhance water security. Nature nanotechnology. 2018; 13(8): 634-641. doi: 10.1038/s41565-018-0203-2
9. Wang G, Fu Y, Ma X, et al. Reusable reduced graphene oxide based double-layer system modified by polyethylenimine for solar steam generation. Carbon. 2017; 114: 117-124. doi: 10.1016/j.carbon.2016.11.071
10. Rezaie K, Mehrpooya M, Delpisheh M, et al. Solar-driven chemisorption cogeneration system integrated with thermal energy storage. Journal of Energy Storage. 2024; 76: 109705. doi: 10.1016/j.est.2023.109705
11. Bai H, Zhao T, Cao M. Interfacial solar evaporation for water production: from structure design to reliable performance. Molecular Systems Design & Engineering. 2020; 5(2): 419-432. doi: 10.1039/C9ME00166B
12. Dao VD, Choi HS. Carbon-based sunlight absorbers in solar-driven steam generation devices. Global Challenges. 2018; 2(2): 1700094. doi: 10.1002/gch2.201700094
13. Ghasemi H, Ni G, Marconnet AM, et al. Solar steam generation by heat localization. Nature Communications. 2014; 5(1): 4449. doi: 10.1038/ncomms5449
14. Carrier O, Shahidzadeh-Bonn N, Zargar R, et al. Evaporation of water: evaporation rate and collective effects. Journal of Fluid Mechanics. 2016; 798: 774-786. doi: 10.1017/jfm.2016.356
15. Eames IW, Marr NJ, Sabir H. The evaporation coefficient of water: A review. International Journal of Heat and Mass Transfer. 1997; 40(12): 2963-2973. doi: 10.1016/S0017-9310(96)00339-0
16. Heymes F, Aprin L, Bony A, et al. An experimental investigation of evaporation rates for different volatile organic compounds. Process Safety Progress. 2013; 32(2): 193-198. doi: 10.1002/prs.11566
17. Manzur A, Cardoso J. Water evaporation rate (Spanish). Revista Mexicana de Física E. 2015; 61(1): 31-34.
18. Sartori E. A critical review on equations employed for the calculation of the evaporation rate from free water surfaces. Solar Energy. 2000; 68(1): 77-89. doi: 10.1016/S0038-092X(99)00054-7
19. Tang R, Etzion Y. Comparative studies on the water evaporation rate from a wetted surface and that from a free water surface. Building and Environment. 2004; 39(1): 77-86. doi: 10.1016/j.buildenv.2003.07.007
20. Turza R, Füri BB. Experimental measurements of the water evaporation rate of a physical model. Slovak Journal of Civil Engineering. 2017; 25(1): 19-23. doi: 10.1515/sjce-2017-0003
21. Örvös M, Szabó V, Poós T. Rate of evaporation from the free surface of a heated liquid. Journal of Applied Mechanics and Technical Physics. 2016; 57: 1108-1117. doi: 10.1134/S0021894416060195
22. Varju E, Poós T. Determination of evaporation rate at free water surface. In: Proceedings of the 8th International Symposium on Exploitation of Renewable Energy Resources and Efficiency (EXPRES 2016); Szabadka, Szerbia.
23. Chiavazzo E, Morciano M, Viglino F, et al. Passive solar high-yield seawater desalination by modular and low-cost distillation. Nature Sustainability. 2018; 1(12): 763-772. doi: 10.1038/s41893-018-0186-x
24. Wang W, Shi Y, Zhang C, et al. Simultaneous production of fresh water and electricity via multistage solar photovoltaic membrane distillation. Nature Communications. 2019; 10(1): 3012. doi: 10.1038/s41467-019-10817-6
25. Xu Z, Zhang L, Zhao L, et al. Ultrahigh-efficiency desalination via a thermally-localized multistage solar still. Energy &

Environmental Science. 2020; 13(3): 830-839. doi: 10.1039/C9EE04122B
26. Yang L, Sun T, Tang J, et al. Photovoltaic-multistage desalination of hypersaline waters for simultaneous electricity, water and salt harvesting via automatic rinsing. Nano Energy. 2021; 87: 106163. doi: 10.1016/j.nanoen.2021.106163
27. Neumann O, Feronti C, Neumann AD, et al. Compact solar autoclave based on steam generation using broadband light-harvesting nanoparticles. Proceedings of the National Academy of Sciences. 2013; 110(29): 11677-11681. doi: 10.1073/pnas.1310131110
28. Zhang Y, Zhao D, Yu F, et al. Floating rGO-based black membranes for solar driven sterilization. Nanoscale. 2017; 9(48): 19384-19389. doi: 10.1039/C7NR06861A
29. Chang C, Tao P, Xu J, et al. High-efficiency superheated steam generation for portable sterilization under ambient pressure and low solar flux. ACS Applied Materials & Interfaces. 2019; 11(20): 18466-18474. doi: 10.1021/acsami.9b04535
30. Li J, Du M, Lv G, et al. Interfacial solar steam generation enables fast-responsive, energy-efficient, and low-cost off-grid sterilization. Advanced Materials. 2018; 30(49): e1805159. doi: 10.1002/adma.201805159
31. Wang Z, Xu L, Liu D, et al. Effects of air temperature and humidity on the kinetics of sludge drying at low temperatures. Energies. 2021; 14(22): 7722. doi: 10.3390/en14227722
32. Finnerty CTK, Menon AK, Conway KM, et al. Interfacial solar evaporation by a 3D graphene oxide stalk for highly concentrated brine treatment. Environmental Science & Technology. 2021; 55(22): 15435-15445. doi: 10.1021/acs.est.1c04010
33. Li X, Li J, Lu J, et al. Enhancement of interfacial solar vapor generation by environmental energy. Joule. 2018; 2(7): 1331-1338. doi: 10.1016/j.joule.2018.04.004
34. Xu X, Ozden S, Bizmark N, et al. A bioinspired elastic hydrogel for solar-driven water purification. Advanced Materials. 2021; 33(18): 2007833. doi: 10.1002/adma.202007833
35. Feistel R, Hellmuth O. Thermodynamics of Evaporation from the Ocean Surface. Atmosphere. 2023; 14(3): 560. doi: 10.3390/atmos14030560
36. Venegas RM, Acevedo J, Treml EA. Three decades of ocean warming impacts on marine ecosystems: A review and perspective. Deep Sea Research Part II: Topical Studies in Oceanography, 2023, 212: 105318. doi: 10.1016/j.dsr2.2023.105318
37. Garcia-Soto C, Cheng L, Caesar L, et al. An overview of ocean climate change indicators: Sea surface temperature, ocean heat content, ocean pH, dissolved oxygen concentration, arctic sea ice extent, thickness and volume, sea level and strength of the AMOC (Atlantic Meridional Overturning Circulation). Frontiers in Marine Science. 2021; 8: 642372. doi: 10.3389/fmars.2021.642372
38. Djellabi R, Noureen L, Dao VD, et al. Recent advances and challenges of emerging solar-driven steam and the contribution of photocatalytic effect. Chemical Engineering Journal. 2022; 431: 134024. doi: 10.1016/j.cej.2021.134024